Metamorphosis of Goldstone and soft fluctuation modes in polariton lasers

R. Binder[1,2] and N. H. Kwong[1]
[1]*Wyant College of Optical Sciences, University of Arizona, Tucson, Arizona 85721, USA*
[2]*Department of Physics, University of Arizona, Tucson, Arizona 85721, USA*

(Received 9 April 2020; revised 22 October 2020; accepted 15 January 2021; published 8 February 2021)

For a driven-dissipative quantum many-body system prepared in a spontaneous broken-symmetry steady state, in addition to the Goldstone mode, the soft fluctuation modes provide important insight into the system's dynamics. Using a microscopic polariton laser theory, we find a rich transformation behavior of discrete and continuum soft modes in a two parameter (pump density and cavity dissipation rate) space. Our theory yields a unified picture of a variety of seemingly disconnected physical concepts including Mott transition, Mollow spectra or relaxation oscillations, polaritonic Bardeen-Cooper-Schrieffer gaps, and Goldstone companion modes. In particular, transformation paths connect the Goldstone companion modes with the Mollow analog modes across a line of exceptional points.

DOI: 10.1103/PhysRevB.103.085304

I. INTRODUCTION

Electrons, holes, and photons in an excited semiconductor microcavity have been studied extensively (e.g., Refs. [1–28]). They form a quantum many-body system that can organize itself into configurations that support coherent order parameters. A semiconductor microcavity laser is a prime example. Being a many-body system with strong photon-matter and Coulomb couplings, it can undergo the lasing transition through more than one physical mechanisms. While the conventional mechanism, with the photons as the main coherent field, is valid for many semiconductor lasers, in some cases lasing is found to be the result of a transition to a state in which polaritons form a nonequilibrium analog of a Bose-Einstein (BEC) or Bardeen-Cooper-Schrieffer (BCS) condensate [18,29–31]. Much insight on these broken-symmetry states can be gained by probing their fluctuation modes. Of particular interest is the Goldstone mode, which is a phase mode of the coherent laser field, and the dissipative modes that are associated with it. It was shown in previous theoretical works on atomic lasers [32] and pumped-dissipative exciton-polariton condensates in quantum-well microcavities [29,33,34] that at zero momentum, the Goldstone mode is accompanied by a damped mode that shares its frequency (here called Goldstone companion mode), and the dispersion of the Goldstone mode at low momentum is diffusive [29,33]. Absent in equilibrium BEC or BCS, this second mode is characteristic of the nonequilibrium character of the laser. It coincides with the Goldstone mode at the lasing threshold and acquires a growing decay rate with further (small) increase in the lasing intensity. Since the laser is a spatially extended many-particle system, it should be expected that the two modes, Goldstone and companion, are in the vicinity, energy-wise, of a large (possibly infinite) number of fluctuation modes with discrete energies or in spectral continua. However, not much is known about this complex landscape of modes and how they transform as external parameters are varied. As we show below, our theoretical analysis provides a unified picture for the transformation of discrete and continuous sets of linear excitation modes, from below threshold (polariton modes and electron-hole continua) to above threshold (Goldstone and companion modes), thus clarifying the relation of seemingly disconnected physical concepts including Mott transition [16], as well as light-induced gaps [35], Mollow-like spectra and sideband emission [13,36–38], polaritonic BCS gaps [29,30], and Goldstone modes [33,34]. Relaxation oscillations in semiconductor lasers [39] have been interpreted as dynamical Stark effect (Mollow) sidebands in Ref. [40], and relaxation oscillations in polariton condensates have been observed [41,42]. Furthermore, we find that above threshold the mode transformations include exceptional points [43].

II. THEORETICAL APPROACH

We use a semiclassical microscopic theory detailed in the Supplemental Material [44] (see, also, Refs. [45,46], and references therein), with electrons, holes, and photons as degrees of freedom, to analyze an incoherently pumped GaAs quantum well inside a microcavity, and to calculate the steady state configurations and their linear response to an interband optical probe.

The fluctuation modes underlying the response are obtained by formulating the response as an eigenvalue problem which is solved numerically. The probe is normal to the quantum well's plane, and hence the probed fluctuations are those of zero wave vector $\mathbf{q}$ in the plane (we do not consider the dispersion of the modes as a function of $\mathbf{q}$).

The eigenvalue set generally consists of continua and discrete modes distributed on the complex energy plane. We follow the evolution of the eigenvalues as we vary the pump density $n_{\rm p}$ and the cavity loss rate $\gamma_{\rm cav}$. The dissipative Goldstone companion mode [29,33,34], alluded to above, is seen

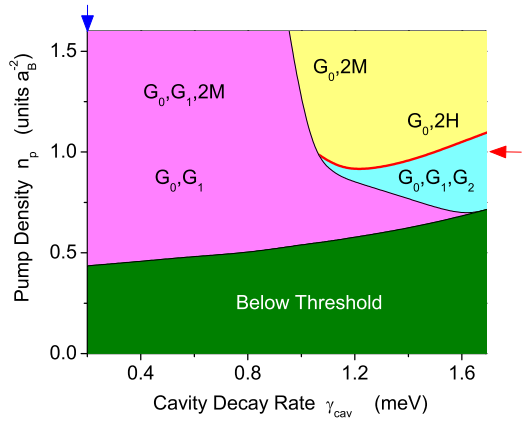

FIG. 1. A map of the discrete modes. Each region is marked by the modes present. Changes in the set of modes occur at the regional boundaries. G_0: Goldstone mode, G_1, G_2: damped modes at the same frequency as G_0, H,M: Mollow analog modes. The meaning of G_1, G_2, H, and M will be clarified in the following figures. Each point on the red curve separating the blue and yellow regions is an exceptional point.

to undergo some nontrivial transformations in this parameter space. At sufficiently high n_p, and sufficiently large γ_{cav}, it meets another laser-frequency, dissipative mode at an exceptional point [43,47–53], where the two modes turn into two others of finite frequency. These latter modes evolve upon further parameter change to Mollow-like modes.

To provide a unifying picture for this and other interesting relations among the subset of discrete soft modes, we show in Fig. 1 a map of the discrete modes. The details of this figure and also the role of continua of modes will become more clear throughout this paper. The response spectra governed by the fluctuation modes are also calculated and shown below. We find the spectral features to be generally consistent with experimental photoluminescence data found in the literature [36,38]. Our fluctuation analysis provides detailed understanding of these spectra and identifies parameter regimes where interesting effects may be observed.

Our theory is based on the semiconductor Bloch equations [39] amended by a single-mode equation for the light field in the cavity E. The equations are of the form $i\hbar\dot{\mathbf{A}} = \mathbf{F}(\mathbf{A})$ where the dynamical variables $\mathbf{A} = (P(\mathbf{k}), f(\mathbf{k}), E)^T$ contain, in addition to E, the complex-valued interband polarization $P(\mathbf{k})$ and real-valued carrier distribution $f(\mathbf{k})$ as a function of wave vector $\mathbf{k}$, and $\mathbf{F}(\mathbf{A})$ is a nonlinear function that contains Coulomb interaction, relaxation, decay, and source (incoherent pump) terms. We solve the equations numerically until steady state is reached. The steady state solution, $\mathbf{A}^{(0)} = (P^{(0)}(\mathbf{k}), f^{(0)}(\mathbf{k}), E^{(0)})^T$ is nonzero above threshold. A small external perturbation field E_{pert} can probe the steady state by inducing small changes $\mathbf{x} = (\delta P(k), \delta P^*(k), \delta f(k), \delta E, \delta E^*)^T$. Linearizing the function $\mathbf{F}(\mathbf{A}^{(0)} + \mathbf{x})$ then yields an equation of the form $i\hbar\dot{\mathbf{x}} = \hat{M}\mathbf{x} + \mathbf{s}_{pert}$ where the complex-valued nonsymmetric matrix M is a nonlinear function of $\mathbf{A}^{(0)}$, and $\mathbf{s}_{pert}$ is proportional to E_{pert}. The right-eigenvalue equation is $\hat{M}\mathbf{x}^{(n)} = \varepsilon^{(n)}\mathbf{x}^{(n)}$. In all the figures displaying eigenvalues, the zero of the real frequency axis is set at the lasing frequency when the system is above the lasing threshold and at the lower polariton (LP) frequency below threshold. We refer to all the discrete modes that oscillate at the laser frequency collectively as G modes, and label them by G_n, $n = 0, 1, 2, ...$, with G_0 being the Goldstone mode. These modes have zero real parts in our plots. We define the complex-valued linear-response function $\chi(\omega) = \delta P_{tot}(\omega)/E_{pert}(\omega)$ where $\delta P_{tot}(\omega) \propto \sum_k \delta P(k, \omega)$.

III. RESULTS AND DISCUSSION

Figure 2 illustrates the evolution of the eigenvalue set as a function of pump density, from near zero to $0.8a_B^{-2}$, for a fixed cavity decay rate of $\gamma_{cav} = 0.2$ meV. Part (a) gives an overview. At vanishing density (C1 in the figure), the eigenvalue set consists of a two-fold degenerate LP mode and a highly degenerate (HD) mode on the imaginary axis, two upper polariton (UP) modes and two spectral (along the real energy direction) continua. The spectral continua show a gap at low frequency due to exciton binding. The modes with nonzero frequency are symmetrically placed. When the system is below threshold, the positive-energy modes are associated with δP, δE, and the negative-energy modes with their complex conjugates. As the pump density n_p increases, the LP modes move up towards zero damping, and the continuum gap closes, ionizing the UP in a Mott transition. As the density crosses the threshold, shown in part (b) to be at $n_p \approx 0.435a_B^{-2}$, the LP modes transform [29,33] to the Goldstone mode G_0 and its damped counterpart G_1, the continuum spectral gap closes completely, and the degenerate HD mode spreads into a decay continuum (along the imaginary energy direction). As the density increases further, the lasing field forces a reopening of the spectral gap via a mechanism similar to that in BCS theory. These trends are shown in more detail in parts (c) and (d). The BCS gap will be further clarified in Fig. 3. Regarding the physical nature of the modes, HD is a pure nonradiative density fluctuation, the decay continuum modes are radiative (involving density, polarization and light field fluctuations), the spectral continua do not contain density oscillations and their polarization oscillations are sharply peaked as a function of k (similar to ionization continuum wave functions of excitons or hydrogen), G_0 (G_1) is a collective mode with a smooth variation of the polarization fluctuation as a function of k and without (with) density fluctuation.

Figures 3(a)–3(d) show the spectral features that emerge at higher pump densities. Parts (a) and (b) compare the response spectra $\mathrm{Im}\chi(\omega)$ at $n_p = 0.8a_B^{-2}$, which is the upper limit in Fig. 2, and $n_p = 3.2a_B^{-2}$. γ_{cav} has the same value as in Fig. 2. The modes underlying the features in the response spectra are shown in Fig. 3(c). A discrete mode, in addition to G_0 and G_1, emerges and becomes separated from the spectral continuum (a discrete mode at the edge of a continuum, rather than inside the continuum, could be called semi-Fano resonance). We label this mode M and identify it as an analog to the Mollow sideband modes (cf. Refs. [13,36,37,40,42]). To support this interpretation, we note that the real part of M's energy, denoted by ε_M, is comparable in value to twice the effective Rabi energy in the rotating-wave approximation $\Delta(\mathbf{k}) = a_c E + \sum_{\mathbf{k}'} V(\mathbf{k} - \mathbf{k}')P(\mathbf{k}')$, where $V(\mathbf{k} - \mathbf{k}')$ is the Coulomb interaction and a_c a coupling constant (see Eq.

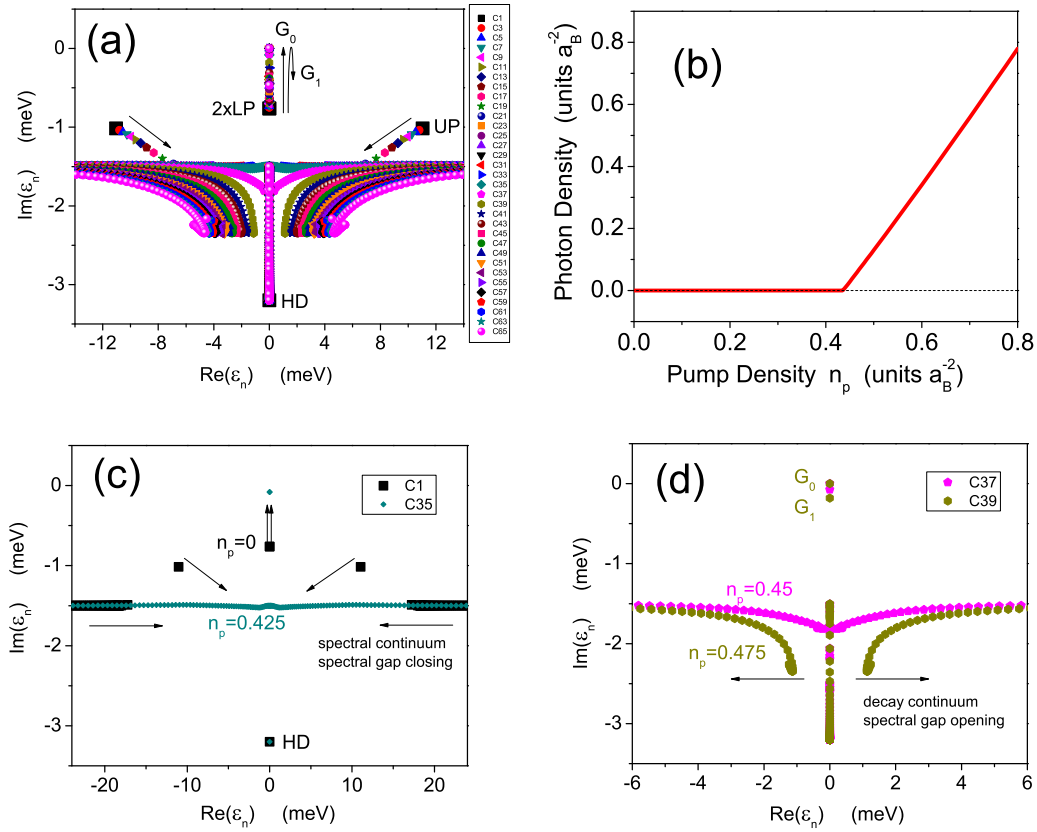

FIG. 2. (a) Eigenenergies obtained from the diagonalization of the linear response matrix $\hat{M}$ for equidistantly spaced pump densities from almost zero, $n_p = 1 \times 10^{-4} a_B^{-2}$, (C1) to $0.8 a_B^{-2}$ (C65), at $T = 50$ K and cavity decay $\gamma_{\rm cav} = 0.2$ meV. Number of k points is $N_k = 300$, linear dimension of $\hat{M}$ is $3N_k + 2$. At zero density we see a damped twofold degenerate lower polariton (LP) state, two upper polariton (UP) states (symmetric above and below LP), and a highly-degenerate (HD) damped state, with a degeneracy of N_k. The arrows indicate the evolution of eigenvalues with increasing pump density. (b) Input-output curve (photon density vs pump density), with threshold approximately at $0.435\, a_B^{-2}$. (c) Same as (a) but only showing two pump densities (almost zero and just below threshold). Spectral gap closing through merging of spectral continua is indicated. (d) Same as (c) for two pump densities just below (above) generation of decay continuum and (BCS-like) spectral gap opening. Here and in all figures showing eigenenergies ε_n, the zero of the real axis is at the LP (below threshold) or the laser frequency (above threshold). The zero of the imaginary axis separates decay ($\mathrm{Im}\varepsilon_n < 0$) from growth ($\mathrm{Im}\varepsilon_n > 0$).

(15) in the Supplemental Material [44]). For example, for $n_{\rm p} = 3.2 a_B^{-2}$, $\varepsilon_{\rm M} = 11.6$ meV, and $2\Delta(\mathbf{k} = \mathbf{0}) = 15$ meV. Note that $\sum_{\mathbf{k}'} V(\mathbf{k} - \mathbf{k}')P(\mathbf{k}')$ is the standard BCS gap function, and $\Delta(\mathbf{k})$ can be viewed as a composite gap function for polariton systems, see, e.g., Ref. [54]. The BCS-like spectral gap grows with $n_{\rm p}$ and its numerical value, marked by the vertical dashed lines, agrees very well with an estimate of the pair-breaking energy $\tilde{E}_{\rm gap}^{\rm pair}$, see Eq. (34) in the Supplemental Material [44]. The lasing field couples the δP, δE components of the perturbed polariton field to their complex conjugates in a manner similar to four-wave mixing (this coupling is absent in linear response below the lasing threshold). The resulting sideband continuum is, as shown in Fig. 3(c), much more pronounced at high $n_{\rm p}$. In parts (a) and (b), the central peaks show the sharp spikes of the Goldstone mode G_0, regularized by a small damping width, and the broader contribution from G_1. To assess the effect of the M modes, we mark the magnitudes of $\varepsilon_{\rm M}$ and $2\Delta(\mathbf{0})$ on the plots. While it is not visible at $n_{\rm p} = 0.8 a_B^{-2}$, the M modes appear to produce features reminiscent of Mollow sidebands in atomic physics at the higher density. This density, $n_{\rm p} = 3.2 a_B^{-2}$, may, however, be too high for experimental verification with stationary lasers. For comparison, we also show in Fig. 3(d) gain spectra calculated for an isolated quantum well, but with the distribution functions obtained from the full calculation in which all G modes are missing (cf. Refs. [54,55]). Far above threshold, they develop signatures of spectral hole burning. In Fig. 3(e) we show a sequence of spectra $|\chi(\omega)|^2$, which is everywhere positive (as are photoluminescence spectra) and allows us to follow the position of the various resonances over a large variation of pump densities. This shows how the Fermi edge absorption grows out of the UP, which was conjectured in Ref. [36], and how the blue shift of the Fermi edge absorption levels off at high densities, consistent with the experimental findings in Ref. [38].

Figures 4(a), and 4(b) in more detail, show the evolution of the eigenvalues for a fixed pump density $n_{\rm p} = 1 a_B^{-2}$ (indicated by the red arrow in Fig. 1) as the cavity decay varies. As $\gamma_{\rm cav}$ increases, G_1 moves down and merges with the decay continuum at $\gamma_{\rm cav} \approx 1.1$ meV. At this point, two modes come out of the continuum acquiring finite frequency. This progression is indicated by the red arrows in part (b). Upon further rise in $\gamma_{\rm cav}$, the Mollow analogs M modes cross over to low frequencies, where we rename the modes as H to indicate that

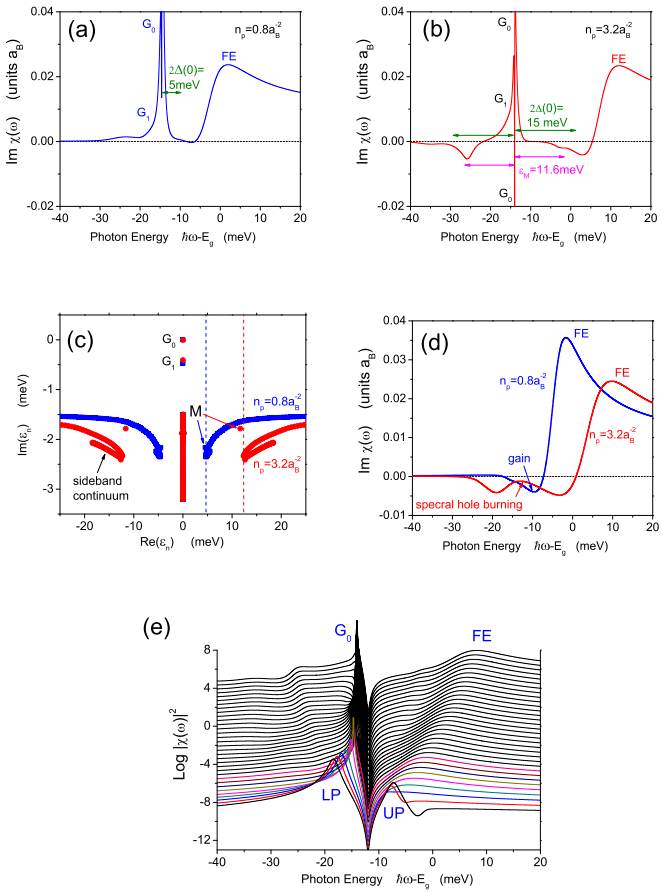

FIG. 3. (a),(b) Calculated linear response spectra, $\mathrm{Im}\chi(\omega)$, for two different pump densities (above and far above threshold). G_0 and G_1 resonances and peak due to Fermi edge (FE) absorption are indicated. BCS-like gap $2\Delta(\mathbf{0})$ (value taken from numerical solution) and Mollow-like states ε_M [value taken from part (c) of this figure] are indicated. (c) Eigenenergies corresponding to spectra in (a),(b). The vertical dashed lines indicate the estimate of the pair excitation gap $\tilde{E}_{\mathrm{gap}}^{\mathrm{pair}}$. (d) For comparison, the spectra obtained from conventional gain-spectra calculations, using same distribution functions as in (a),(b) but without coherent light and interband polarization fields. (e) Calculated linear response spectra, $|\chi(\omega)|^2$, for pump densities equidistantly spaced from almost zero to $n_p = 3.2a_B^{-2}$. Except for the lowest pump density, the spectra are shifted vertically for clarity. For clarity, the Fourier transform from time to frequency contains an additional phenomenological broadening $\gamma_a = 0.04$ meV, since the Goldstone mode would diverge otherwise.

the modes' characteristics have changed. As indicated by the black arrows in part (b), the two H modes meet at an exceptional point [43,47–53], where the two eigenvectors become one state which is self-orthogonal with respect to the inner product using right and left eigenvectors, and turn into two G modes, G_1 moving up the imaginary axis and G_2 moving down. The bottom panels of Fig. 4 show the generation of the H/M modes as density increases by a transformation from G_1 and G_2 at an exceptional point Fig. 4(c)] and by separating from the spectral continuum [Fig. 4(d)]. In order to identify the exceptional point in our numerical analysis, we applied three numerical criteria. First, we zoomed-in, so to speak, closer and closer to the annihilation-creation point and find no signatures of anticrossing, which is associated with usual degeneracy. Second, we also tested the self-orthogonality, and find that it improves as we zoom in to the point (in any practical numerical calculation, the norm of an eigenvector can become small but cannot assume a value of exactly zero). Third, we verified that there is only one eigenfunction for the two states.

As noted above, we have performed the eigenvalue computation over a region of the $(\gamma_{\mathrm{cav}}, n_{\mathrm{p}})$ parameter plane and constructed a map of discrete fluctuation modes shown in Fig. 1. The lines separate regions of different numbers of discrete G modes (unlike lines in phase diagrams that separate regions of different numbers of stable and unstable solutions to a nonlinear set of equations). The specific cases discussed above are instances on this diagram: the blue arrow marks the cases in Figs. 2 and 3(a)–3(c) and the red arrow marks the cases in Figs. 4(a) and 4(b). The three (color-coded) regions above the lasing threshold are defined and labeled by the Goldstone and discrete soft modes that are present, and some modes are transformed when a curve between two regions is crossed. The (red) curve separating the blue and yellow regions is made up of exceptional points at which G_1 and G_2 meet and turn into two H modes or vice versa, as illustrated in Figs. 4(a) and 4(b) and in detail in 4(c). In the pink region, as n_{p} increases from the lasing threshold, G_1 separates from the Goldstone mode G_0 and moves down along the imaginary axis in the complex energy plane. When the boundary curve with the blue region is crossed, the mode G_2 emerges from the decay continuum and moves up towards G_1 along this axis. G_2 does not appear at small γ_{cav}, and at the curve marking the crossing from the pink region to the yellow region, G_1 merges with the decay continuum and ceases to be a distinct mode.

The steady state solutions for $\gamma_{\mathrm{cav}} = 0.2$ meV, at the left boundary in Fig. 1, have been discussed in Ref. [30]. Above the threshold, they can be classified as polariton-BCS states. With increasing γ_{cav}, the states above threshold gradually and smoothly depart from the polariton-BCS state at $\gamma_{\mathrm{cav}} = 0.2$ meV. For the range shown in the figure, they become more similar, but do not fully reach the photon-laser case, because their emission frequencies remain about 2 meV below the cavity resonance, and the distribution function at $k = 0$, which is 0.57 in the polariton-BCS case of $\gamma_{\mathrm{cav}} = 0.2$ meV, increases only to 0.72 at $\gamma_{\mathrm{cav}} = 1.2$ meV, and stays below Fermi degeneracy, defined as $f(0) = 1$, at the right boundary of the figure, i.e., at $\gamma_{\mathrm{cav}} = 1.7$ meV, where $f(0) = 0.8$ at threshold and $f(0) = 0.82$ at the red EP line [56].

IV. CONCLUSION

In summary, we have studied in detail the low-frequency fluctuation modes of an incoherently-pumped polariton laser at the long-wavelength limit. The set of mode eigenvalues generally consists of both continuous and discrete subsets in the complex energy plane. Tracing the evolution of this eigenvalue set when two parameters (pump density and cavity loss rate) vary, reveals interesting features. The onset of lasing spreads a highly degenerate dissipative mode into a decay continuum along the imaginary energy axis. Further increase in pump density creates a new sideband continuum. The behavior of the discrete subset is summarized in a phase

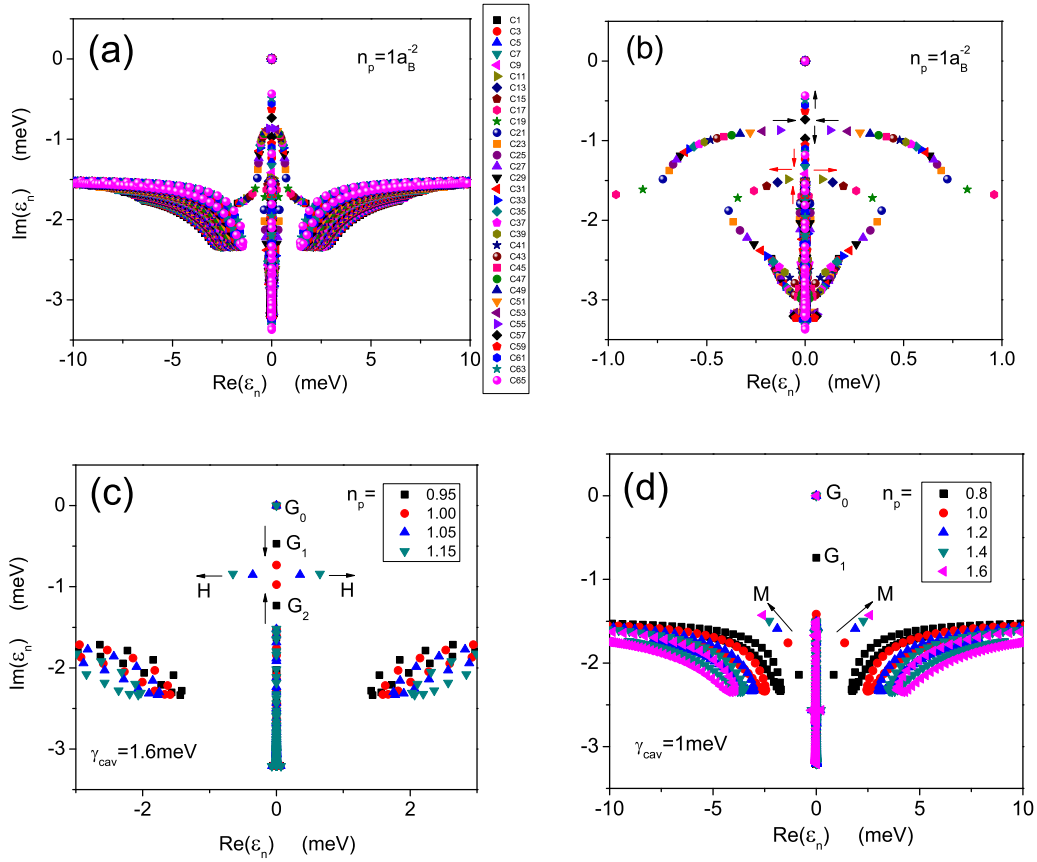

FIG. 4. (a) Eigenenergies for equidistantly spaced cavity rates γ_{cav} from 0.9 meV (C1) to 1.7 meV (C65) at fixed pump density $n_p = 1a_B^{-2}$. (b) Same as (a) but zoomed in to smaller frequency interval. The arrows indicate the evolution of eigenvalues with increasing decay rates. The transformation marked by the red arrows happens at a lower γ_{cav} than that marked by the black arrows. In the transformation indicated by the black arrows, the two converging modes meet at an exceptional point. (c) Collision, as n_p increases, of two damped G modes (G_2, G_3) at an exceptional point generating two H modes. (d) Example of Mollow-like modes (M) rising above decay continuum.

diagram in the (n_p, γ_{cav}) parameter space (Fig. 1). A curve of exceptional points are present which link the Goldstone companion G_1 to Mollow modes. The overall picture of the low-frequency fluctuation modes that we have found here may also be more generally applicable to other lasers and driven quantum symmetry-broken systems, e.g., Refs. [57–60]. We finally note that all figures in our manuscript present physical observables and thus can, in principle, be directly measured in experiments. This, in particular, includes the signatures of the exceptional point: there is no avoided crossing in the plane of the complex eigenenergies. In an experimental study of an atomic cavity [61] the complex emission energies of an atomic cavity have been directly observed from those measurements and the critical behavior of the exceptional point, including its topological properties, inferred. Similar measurements are, in principle' possible in the our case, although the details of the experiment would be more complicated. Our exceptional point is at the frequency of the condensate, and there is a continuum of more strongly damped modes at the same frequency. Hence, a careful line-shape analysis would be needed to isolate the effects of the exceptional point. Furthermore, the continuous variation of the cavity decay time may be more difficult to implement in the semiconductor cavity.

ACKNOWLEDGMENTS

We gratefully acknowledge financial support from the U.S. National Science Foundation (NSF) under Grant No. DMR 1839570, and CPU time at HPC, University of Arizona.

[1] X. Fan, H. Wang, H. Q. Hou, and B. E. Hammons, Phys. Rev. A **56**, 3233 (1997).

[2] H. Cao, S. Pau, J. M. Jacobson, G. Björk, Y. Yamamoto, and A. Imamŏglu, Phys. Rev. A **55**, 4632 (1997).

[3] M. Kuwata-Gonokami, S. Inouye, H. Suzuura, M. Shirane, R. Shimano, T. Someya, and H. Sakaki, Phys. Rev. Lett. **79**, 1341 (1997).

[4] M. Kira, F. Jahnke, W. Hoyer, and S. W. Koch, Prog. Quantum Electron. **23**, 189 (1999).

[5] S. A. Moskalenko and D. W. Snoke, *Bose-Einstein Condensation of Excitons and Biexcitons and Coherent Nonlinear Optics with Excitons* (Cambridge University Press, Cambridge, 2000).

[6] C. Ciuti, P. Schwendimann, B. Deveaud, and A. Quattropani, Phys. Rev. B **62**, R4825 (2000).

[7] P. G. Savvidis, J. J. Baumberg, R. M. Stevenson, M. S. Skolnick, D. M. Whittaker, and J. S. Roberts, Phys. Rev. Lett. **84**, 1547 (2000).

[8] N. H. Kwong, R. Takayama, I. Rumyantsev, M. Kuwata-Gonokami, and R. Binder, Phys. Rev. Lett. **87**, 027402 (2001).

[9] J. J. Baumberg and P. G. Lagoudakis, Phys. Stat. Solidi B **242**, 2210 (2005).

[10] J. Keeling, F. M. Marchetti, M. H. Szymanska, and P. B. Littlewood, Semicond. Sci. Technol. **22**, R1 (2007).

[11] S. Schumacher, N. H. Kwong, and R. Binder, Phys. Rev. B **76**, 245324 (2007).

[12] D. Bajoni, P. Senellart, E. Wertz, I. Sagnes, A. Miard, A. Lemaître, and J. Bloch, Phys. Rev. Lett. **100**, 047401 (2008).

[13] J. Berney, M. T. Portella-Oberli, and B. Deveaud, Phys. Rev. B **77**, 121301(R) (2008).

[14] A. Amo, D. Sanvitto, F. P. Laussy, D. Ballarini, E. del Valle, M. D. Martin, A. Lemaitre, J. Bloch D. N. Krizhanovskii, M. S. Skolnick, C. Tejedor, and L. Vina, Nature (London) **457**, 291 (2009).

[15] D. Sanvitto and V. Timofeev, *Exciton Polaritons in Microcavities* (Springer, Berlin, 2012).

[16] D. Semkat, F. Richter, D. Kremp, G. Manzke, W. D. Kraeft, and K. Henneberger, Phys. Rev. B **80**, 155201 (2009).

[17] K. Kamide and T. Ogawa, Phys. Rev. Lett. **105**, 056401 (2010).

[18] H. Deng, H. Haug, and Y. Yamamoto, Rev. Mod. Phys. **82**, 1489 (2010).

[19] D. Snoke and P. Littlewood, Phys. Today **63**, 42 (2010).

[20] X. Liu and T. Galfsky and Zh. Sun and F. Xia and E. Lin and Y. Lee and S. Kena-Cohen and V. Menon, Nat. Photonics **9**, 30 (2014).

[21] F. Schulze, B. Lingnau, S. M. Hein, A. Carmele, E. Scholl, K. Ludge, and A. Knorr, Phys. Rev. A **89**, 041801(R) (2014).

[22] J. M. Menard, C. Poellmann, M. Porer, U. Leierseder, E. Galopin, A. Lemaitre, A. Amo, J. Bloch, and R. Huber, Nat. Commun. **5**, 4648 (2014).

[23] M. K. Dezfouli, M. M. Dignam, M. J. Steel, and J. E. Sipe, Phys. Rev. A **90**, 043832 (2014).

[24] J. Schmutzler, P. Lewandowski, M. Assmann, D. Niemietz, S. Schumacher, M. Kamp, C. Schneider, S. Hofling, and M. Bayer, Phys. Rev. B **91**, 195308 (2015).

[25] A. W. de Leeuw, E. C. I. van der Wurff, R. A. Duine, D. van Oosten, and H. T. C. Stoof, Phys. Rev. A **94**, 013615 (2016).

[26] W. Hayenga and M. Khajavikhan, Light: Sci. Appl. **6**, e17091 (2017).

[27] A. V. Kavokin, J. J. Baumberg, G. Malpuech, and F. P. Laussy, *Microcavities* (Oxford Science Publications, London, 2017).

[28] W. Bao, Xiaoze Liu, Fei Xue, Fan Zheng, Renjie Tao, Siqi Wang, Yang Xia, Mervin Zhao, Jeongmin Kim, Sui Yang, Quanwei Li, Ying Wang, Yuan Wang, L.-W. Wang, A. H. MacDonald, and X. Zhang, Proc. Natl. Acad. Sci. USA **116**, 20274 (2019).

[29] M. H. Szymanska, J. Keeling, and P. B. Littlewood, Phys. Rev. Lett. **96**, 230602 (2006).

[30] J. Hu, Z. Wang, S. Kim, H. Deng, S. Brodbeck, C. Schneider, S. Höfling, N. H. Kwong, and R. Binder, Phys. Rev. X **11**, 011018 (2021).

[31] H. Hu and X.-J. Liu, Phys. Rev. A **101**, 011602(R) (2020).

[32] K. Chou and Z. Su, Prog. Theor. Phys. Supp. **86**, 34 (1986).

[33] M. Wouters and I. Carusotto, Phys. Rev. Lett. **99**, 140402 (2007).

[34] R. Hanai, P. B. Littlewood, and Y. Ohashi, Phys. Rev. B **97**, 245302 (2018).

[35] V. M. Galitskii, S. P. Goreslavskii, and V. F. Elesin, Zh. Eksp. Teor. Fiz. **57**, 207 (1970) [Sov. Phys. JETP **30**, 117 (1970)].

[36] F. Quochi, G. Bongiovanni, A. Mura, J. L. Staehli, B. Deveaud, R. P. Stanley, U. Oesterle, and R. Houdre, Phys. Rev. Lett. **80**, 4733 (1998).

[37] T. Byrnes, T. Horikiri, N. Ishida, and Y. Yamamoto, Phys. Rev. Lett. **105**, 186402 (2010).

[38] T. Horikiri, M. Yamaguchi, K. Kamide, Y. Matsuo, T. Byrnes, N. Ishida, A. Löffler, S. Höfling, Y. Shikano, T. Ogawa, A. Forchel, and Y. Yamamoto, Sci. Rep. **6**, 25655 (2016).

[39] W. W. Chow, S. W. Koch, and M. Sargent III, *Semiconductor-Laser Physics* (Springer, Berlin, 1994).

[40] B. Thedrez and R. Frey, Opt. Lett. **13**, 105 (1988).

[41] M. De Giorgi, Dario Ballarini, Paolo Cazzato, George Deligeorgis, Simos I. Tsintzos, Zacharias Hatzopoulos, Pavlos G. Savvidis, Giuseppe Gigli, F. P. Laussy, and D. Sanvitto, Phys. Rev. Lett. **112**, 113602 (2014).

[42] T. Horikiri, Kenichiro Kusudo, Michael D. Fraser, Y. Matsuo, Andreas Löffler, Sven Höfling, Alfred Forchel, and Y. Yamamoto, J. Phys. Soc. Jpn. **87**, 094401 (2018).

[43] W. D. Heiss, J. Phys. A Math. Gen. **37**, 2455 (2004).

[44] See Supplemental Material at http://link.aps.org/supplemental/10.1103/PhysRevB.103.085304 for a detailed description of the theory, the constituent equations of motion for the interband polarization, carrier distribution functions and light field cavity-mode equations, as well as the linear response theory based on those equations.

[45] B. Gu, N. H. Kwong, and R. Binder, Phys. Rev. B **87**, 125301 (2013).

[46] R. Binder and S. W. Koch, Prog. Quantum Electron. **19**, 307 (1995).

[47] C. Dembowski, H.-D. Gräf, H. L. Harney, A. Heine, W. D. Heiss, H. Rehfeld, and A. Richter, Phys. Rev. Lett. **86**, 787 (2001).

[48] M. Liertzer, L. Ge, A. Cerjan, A. D. Stone, H. E. Tureci, and S. Rotter, Phys. Rev. Lett. **108**, 173901 (2012).

[49] T. Gao, E. Estrecho1, K. Y. Bliokh, T. C. H. Liew, M. D. Fraser, S. Brodbeck, M. Kamp, C. Schneider, S. Hoefling, Y. Yamamoto, F. Nori, Y. S. Kivshar, A. G. Truscott, R. G. Dall, and E. A. Ostrovskay, Nature (London) **526**, 554 (2015).

[50] R. Hanai, A. Edelman, Y. Ohashi, and P. B. Littlewood, Phys. Rev. Lett. **122**, 185301 (2019).

[51] R. Hanai and P. B. Littlewood, Phys. Rev. Research **2**, 033018 (2020).

[52] M. A. Miri and A. Alu, Sci. Mag. **363**, eaar7709 (2019).

[53] M. Sakhdari, M. Hajizadegan, Q. Zhong, D. N. Christodoulides, R. El-Ganainy, and P. Y. Chen, Phys. Rev. Lett. **123**, 193901 (2019).

[54] M. Yamaguchi, K. Kamide, R. Nii, T. Ogawa, and Y. Yamamoto, Phys. Rev. Lett. **111**, 026404 (2013).

[55] M. Yamaguchi, R. Nii, K. Kamide, T. Ogawa, and Y. Yamamoto, Phys. Rev. B **91**, 115129 (2015).

[56] In the parameter regime explored in this study we do not observe any phase transitions and/or exceptional points predicted in Ref. [50]. See also Ref. [51].
[57] C. Zh. Ning and H. Haken, Phys. Rev. A **41**, 3826 (1990).
[58] S. Ebata, T. Nakatsukasa, Tsunenori Inakura, Kenichi Yoshida, Yukio Hashimoto, and K. Yabana, Phys. Rev. C **82**, 034306 (2010).
[59] Y. Hama, G. Tsitsishvili, and Z. F. Ezawa, Prog. Theor. Exp. Phys. **2013**, 053I01 (2013).
[60] S. Hannibal, P. Kettmann, M. D. Croitoru, V. M. Axt, and T. Kuhn, Phys. Rev. A **97**, 013619 (2018).
[61] Y. Choi, S. Kang, Sooin Lim, Wookrae Kim, J.-R. Kim, J.-H. Lee, and K. An, Phys. Rev. Lett. **104**, 153601 (2010).